Tellus SERIES A DYNAMIC METEOROLOGY AND OCEANOGRAPHY
PUBLISHED BY THE INTERNATIONAL METEOROLOGICAL INSTITUTE IN STOCKHOLM

Tellus (2010), 62A, 71–79
Printed in Singapore. All rights reserved

TELLUS

Energetics of tidally generated internal waves for nonuniform stratification

By MOUNDHEUR ZARROUG*, JONAS NYCANDER and KRISTOFER DÖÖS, *Department of Meteorology, Stockholm University, 106 91 Stockholm, Sweden*

(Manuscript received 16 February 2009; in final form 14 August 2009)

ABSTRACT

The generation of internal waves from barotropic tides can be quantified in terms of the conversion rates. These have often been obtained by applying the WKB approximation, which yields an expression for the conversion rates which is proportional to the seabed buoyancy frequency N_B. For small values of N_B or strong variations of the buoyancy profile $N(z)$, this gives unreliable results. Using homogenization theory it is here shown that the conversion rate instead depends on the value of $N(z)$ averaged over a vertical region at the bottom of the same magnitude as the vertical length-scale of the internal wave, which for the lowest modes is of the same order as the entire ocean depth. This gives a substantially larger conversion rate.

1. Introduction

While bottom friction is considered to be the main reason for the tidal dissipation of energy in shallow waters, the picture is different when the deep ocean is concerned. Here internal waves generated by barotropic tides provide the main mechanism for the dissipation (Egbert and Ray, 2000, 2001), and account for the main energy source needed to maintain vertical mixing in the ocean (Munk and Wunsch, 1998). Without this mixing, the ocean would become a stagnant pool (Sandström, 1908), and it is therefore of critical importance both for global thermohaline circulation (Nilsson et al., 2003) and for oceanic biology (Andrews and Gentien, 1982; Leichter et al., 1998).

The theoretical models used to determine the energy converted from the tides to the internal gravity wavefield are often based on the WKB approximation in the vertical (Llewellyn Smith and Young, 2002; Nycander, 2005). However, as will be shown here, this approximation typically gives large errors for the gravest modes. In many cases the two first modes are important; in particular, they are the ones mainly responsible for transporting wave energy large distances from the generation site (Alford, 2003). Also, the WKB approximation yields conversion rates which are dependent upon the buoyancy frequency at the seabed. Here strong mixing will give rise to an abrupt decrease of the buoyancy frequency (Ledwell et al., 2000), yielding conversion rates which spuriously tend towards small values. A better understanding of how the internal-wave generation depends on the vertical density profile is thus desirable.

We will start in Section 2 by describing the physical model to be used in the present study. Section 3 provides a short review of WKB theory. Section 4 will deal with homogenization theory as an alternative to the standard WKB approximation, whereafter the main results of our analysis are given in Section 5. The study is concluded in Section 6 by a discussion of its overall results.

2. The physical model

The original formulation of the problem is due to Bell (1975a, b), who postulated an infinitely deep ocean with a constant stratification. Subsequent studies by Llewellyn Smith and Young (2002) and Khatiwala (2003) broadened the scope of the model by assuming a finite oceanic depth and incorporating an arbitrary density profile (represented by $N(z)$, the vertical distribution of the buoyancy frequency).

In this study, we will restrict ourselves to topographies $h(x)$ with the specific shape

$$h(x) = \frac{h_0}{1 + (\frac{x}{\Lambda})^2}, \tag{1}$$

where Λ is the width of the ridge. The associated Fourier transform is

$$\tilde{h}(\kappa) = h_0 \Lambda \pi \exp(-|\kappa|\Lambda), \tag{2}$$

κ being the wavenumber. The symmetry of the one-dimensional topography with an infinite extent along the y-axis affects the generation of internal waves in such manner that the only

*Corresponding author.
e-mail: zarroug@misu.su.se
DOI: 10.1111/j.1600-0870.2009.00415.x

contributions to the wave generation come from the tidal velocity component along the x-axis. The barotropic tidal velocity of frequency ω_0 is therefore assumed to be

$$\vec{U} = U_0 \vec{x} \cos(\omega_0 t). \tag{3}$$

The investigation is restricted to the acoustic limit, *viz.* $U_0/\Lambda\omega_0 < 1$. In this limit the advective terms, for example, $\vec{v}\Delta\vec{v}$, can be neglected, as was done by (Llewellyn Smith and Young, 2002). The problem is also linearized by expanding the kinematic boundary condition at the bottom, with the topographic height h_0 used as expansion parameter. This is acceptable as long as one considers subcritical topographies, defined by $N_B h/\Lambda\omega_0 < 1$, where N_B is the Brunt-Väisälä frequency at the seabed.

2.1. The vertical structure

In this subsection, we will present the full analytical expression for the conversion rates in an ocean of finite depth H and with a topography specified by eq. (1). This will be done without using any approximation of the function $N(z)$. Following Llewellyn Smith and Young (2002), the vertical structure of the propagating waves is given by the eigenfunctions Ψ_n satisfying the following Sturm-Liouville problem:

$$\frac{\mathrm{d}}{\mathrm{d}z}\left[\frac{1}{N(z)^2}\frac{\mathrm{d}\Psi_n}{\mathrm{d}z}\right] + \frac{1}{c_n^2}\Psi_n = 0, \tag{4}$$

where c_n is the nth eigenvalue. The eigenfunctions Ψ_n satisfy the boundary conditions

$$\frac{\mathrm{d}\Psi_n(z)}{\mathrm{d}z}(0) = \frac{\mathrm{d}\Psi_n(z)}{\mathrm{d}z}(-H) = 0, \tag{5}$$

and furthermore the orthogonality relation

$$\int_{-H}^{0} \Psi_n(z)\Psi_m(z)\mathrm{d}z = \frac{A_n}{\lambda_n}\delta_{mn}, \tag{6}$$

where A_n is a normalization constant, δ_{mn} a Kronecker matrix, and $\lambda_n = c_n/f_0$ the Rossby radius (f_0 being the Coriolis parameter). We define

$$\kappa_n = \frac{\sqrt{\omega_0^2 - f_0^2}}{c_n} \tag{7}$$

as the modal horizontal wavenumber. The horizontal velocity field as well as the pressure are expanded in these eigenfunctions

$$(u, v, p) = \sum_{n=1}^{\infty} \lambda_n [u_n(x, y, t), v_n(x, y, t), p_n(x, y, t)]\Psi_n(z). \tag{8}$$

The problem is then solved by projecting the equations of motion on this set of eigenfunctions. This was by by Llewellyn Smith and Young (2002), using the linearized, rotating and hydrostatic equations. In this way, they derived the following modal conversion rate:

$$\mathcal{C}_n^{\text{exact}} = \frac{\rho_0\omega_0^2 U_0^2 L}{4 f_0}\left(1 - \frac{f_0^2}{\omega_0^2}\right)^{3/2} \frac{|\,\tilde{h}(\kappa_n)\,|^2\,\Psi_n^2(-H)}{A_n}, \tag{9}$$

where ρ_0 is the average oceanic density and L the length of the ridge in the y-direction (assumed to be much greater than the width of the ridge). Note that the buoyancy-frequency profile $N(z)$ is arbitrary. The total conversion rate is obtained by summation over the entire spectrum

$$\mathcal{C} = \sum_{n=1}^{\infty} \mathcal{C}_n. \tag{10}$$

$\mathcal{C}_n$ and $\mathcal{C}$ obtained by numerical integration of eq. (4) will in what follows be referred to as 'exact' or 'numerical' results.

3. The WKB approximation

If $N(z)$ varies more slowly than the eigenfunctions Ψ_n, the WKB approximation can be used (Morse and Feshbach, 1953; Bender and Orszag, 1978). To lowest order, this procedure yields the following approximate solution:

$$\Psi_n \simeq \sqrt{\frac{N(z)}{\overline{N}}}\frac{n\pi}{H}\cos\left[\frac{n\pi}{H\overline{N}}\int_{-H}^{z} N(z')\,\mathrm{d}z'\right], \tag{11}$$

and

$$c_n \simeq \frac{H\overline{N}}{n\pi}, \tag{12}$$

where

$$\overline{N} = \frac{\int_{-H}^{0} N(z)\,\mathrm{d}z}{H}. \tag{13}$$

The wavenumber, cf. eq. (7), becomes

$$\kappa_n \simeq \sqrt{\omega_0^2 - f_0^2}\frac{n\pi}{H}. \tag{14}$$

The orthogonality relation, on the other hand, assumes the form

$$\int_{-H}^{0} \Psi_n(z)\Psi_m(z)\mathrm{d}z \simeq \frac{n^2\pi^2}{2H}\delta_{mn}, \tag{15}$$

in which case the normalization constant becomes

$$A_n = \frac{n\pi\overline{N}}{2 f_0}. \tag{16}$$

These simplifications lead us to reconsider the expression for the modal conversion rate, which can be recast in the following form:

$$\mathcal{C}_n^{\text{WKB}} = \frac{\rho_0 U_0^2 L N_B}{2\pi}\sqrt{1 - \frac{f_0^2}{\omega_0^2}}\tilde{h}(\kappa_n)\tilde{h}^*(\kappa_n)\kappa_n\delta\kappa, \tag{17}$$

where the star denotes complex conjugate, and

$$\delta\kappa = \frac{\kappa_n}{n}. \tag{18}$$

For the particular ridge topography in eq. (1) the Fourier transform $\tilde{h}$ is given by eq. (2). The total conversion rate is then obtained as the sum of all the modal conversion rates,

$\mathcal{C}^{\mathrm{WKB}} = \Sigma_{n=1}^{\infty}\mathcal{C}_n^{\mathrm{WKB}}$, namely,

$$\mathcal{C}^{\mathrm{WKB}} = \frac{\rho_0 U_0^2 h_0^2 L N_B \gamma}{2\pi}\sqrt{1-\frac{f_0^2}{\omega_0^2}}\sum_{n=1}^{\infty} n\gamma \exp(-2n\gamma), \tag{19}$$

where $\gamma = \Lambda\delta\kappa$. This expression, derived using WKB theory, shows a dependence of the total conversion rate on the seabed value of the buoyancy frequency, N_B. This gives rise to problems, since turbulence may lead to a decrease of the buoyancy frequency near the bottom.

We finally define the ratio between the conversion rates calculated from the full analytical solution and from the WKB approximation, that is,

$$R_n^{\mathrm{WKB}} = \frac{\mathcal{C}_n^{\mathrm{WKB}}}{\mathcal{C}_n^{\mathrm{exact}}}. \tag{20}$$

In order to evaluate $\mathcal{C}_n^{\mathrm{exact}}$, eq. (4) must be integrated numerically to provide $\Psi_n(-H)$.

The assumptions that $H \to \infty$ and $\delta\kappa \to 0$ (alternatively $\Lambda \to 0$) lead to the continuous energy spectrum derived by Bell (1975b). Taking the limit $\delta\kappa \to 0$ allows us to transform the sum of the discrete modal conversion rates defined by eq. (10) to an integration over the continuous spectrum of wavenumbers κ

$$\sum_{n=1}^{\infty}\mathcal{C}_n^{\mathrm{WKB}} \to \int_0^{\infty}\mathcal{C}_n^{\mathrm{WKB}}\mathrm{d}\kappa. \tag{21}$$

The following definition is now introduced:

$$\mathcal{C}_{\mathrm{Bell}}^{\mathrm{WKB}} = \int_0^{\infty}\mathcal{C}_n^{\mathrm{WKB}}d\kappa = \frac{\rho_0 U_0^2 L N_B}{2\pi}\sqrt{1-\frac{f_0^2}{\omega_0^2}}\int_0^{\infty}\tilde{h}(\kappa)\tilde{h}^*(\kappa)\kappa\,\mathrm{d}\kappa, \tag{22}$$

where $\mathcal{C}_{\mathrm{Bell}}^{\mathrm{WKB}}$ can be seen as equivalent to the value of $\mathcal{C}^{\mathrm{WKB}}$ in the limit $\Lambda \to 0$. Evaluating the integral for the topography given by eq. (1) yields the final result

$$\mathcal{C}_{\mathrm{Bell}}^{\mathrm{WKB}} = \frac{\pi}{8}\rho_0 U_0^2 h_0^2 L N_B\sqrt{1-\frac{f_0^2}{\omega_0^2}}. \tag{23}$$

These 'Narrow-ridge' topographies (Λ 'small') mainly interact with high-frequency waves. In these cases the eigenfunction Ψ_n will vary more rapidly than $N(z)$, and thus WKB theory is expected to be valid and very precise in this limit.

4. Homogenization theory

As discussed in the introduction, a number of complications arise when the prerequisites for the validity of the WKB approximation (cf. Section 3) are not fulfilled, above all that the straightforward dependence of the conversion upon the value of N_B no longer holds (a topic to be dealt with in greater detail in Section 5). In these cases we need to adopt another strategy. In the new approach we assume that the buoyancy frequency profile has variations on two different length scales, and the basic idea is to average out the rapid variations. This can be done in a consistent way if these rapid variations have a shorter length scale than the vertical wavelength of the internal wave mode.

We first reformulate eq. (4) as

$$\frac{\mathrm{d}^2\psi_n(z)}{\mathrm{d}z^2} + \frac{N^2(z)}{c_n^2}\psi_n(z) = 0, \tag{24}$$

where

$$\frac{\mathrm{d}\psi_n(z)}{\mathrm{d}z} = \Psi_n(z), \tag{25}$$

and the boundary conditions for ψ_n are

$$\psi_n(0) = \psi_n(-H) = 0. \tag{26}$$

These expressions will serve as the starting-point for our analysis.

We will now attempt to decompose the original problem given by eq. (24) into a two-scale problem, based on a short length-scale which does justice to the rapid variations of the buoyancy-frequency profile, and a long length-scale over which $N(z)$ remains constant (or at least only varies slowly). The buoyancy-frequency profile will thus be regarded as the sum of a mean value (associated with the long scale), and another component which oscillates on the short scale. We assume that the variables α and β are associated with the slow and fast variations, respectively, and that $\epsilon = \frac{\alpha}{\beta}$ is a small parameter. The wavefunction may then be written formally as

$$\psi_n(z) = \psi_n[\alpha(z), \beta(z)], \tag{27}$$

and the buoyancy-frequency profile as

$$N(z) = N[\alpha(z), \beta(z)], \tag{28}$$

where

$$\alpha = z, \quad \beta = \frac{z}{\epsilon}. \tag{29}$$

The total derivative with respect to z can thus be written as

$$\frac{\mathrm{d}}{\mathrm{d}z} = \frac{\mathrm{d}\alpha}{\mathrm{d}z}\partial_\alpha + \frac{\mathrm{d}\beta}{\mathrm{d}z}\partial_\beta = \partial_\alpha + \frac{1}{\epsilon}\partial_\beta, \tag{30}$$

whereafter eq. (24) becomes

$$\left(\partial_\alpha + \frac{1}{\epsilon}\partial_\beta\right)^2\psi_n + \frac{N^2}{c_n^2}\psi_n(\alpha,\beta) = 0, \tag{31}$$

in turn leading to

$$\left[\partial_\alpha^2 + \frac{N^2(\alpha,\beta)}{c_n^2} + \frac{1}{\epsilon}2\partial_\alpha\partial_\beta + \frac{1}{\epsilon^2}\partial_\beta^2\right]\psi_n(\alpha,\beta) = 0. \tag{32}$$

The wavefunction is now expanded in powers of ϵ

$$\psi_n(\alpha,\beta) = \sum_{i=0}^{\infty}\epsilon^i\psi_n^{(i)}, \tag{33}$$

and hereafter inserted in eq. (32). Equating terms of equal powers in ϵ yields the following hierarchy of differential equations:

$$\epsilon^0 : \tilde{O}_0\psi_n^{(0)} = 0, \tag{34}$$

$$\epsilon^1 : \tilde{O}_1\psi_n^{(0)} + \tilde{O}_0\psi_n^{(1)} = 0, \tag{35}$$

$$\epsilon^2 : \tilde{O}_2\psi_n^{(0)} + \tilde{O}_1\psi_n^{(1)} + \tilde{O}_0\psi_n^{(2)} = 0, \tag{36}$$

where

$$\tilde{O}_0 = \partial_\beta^2, \tag{37}$$

$$\tilde{O}_1 = 2\partial_\alpha\partial_\beta, \tag{38}$$

$$\tilde{O}_2 = \partial_\alpha^2 + \frac{N^2}{c_n^2}. \tag{39}$$

We start by examining eq. (34) and recognize that mathematically a linear solution is possible

$$\psi_n^{(0)} = \beta A + u_n^{(0)}(\alpha). \tag{40}$$

From a physical standpoint the presence of the linear term in β is, however, precluded since the zeroth-order wavefunction must be bounded as $\epsilon \to 0$, and hence $\beta \to \infty$. Hence the only acceptable solution is

$$\psi_n^{(0)} = u_n^{(0)}(\alpha). \tag{41}$$

This implies that the zeroth-order solution remains independent of the small scale, or in other words, of the rapid variations of the buoyancy profile. Insertion of this solution into eq. (35) leads to

$$\tilde{O}_0\psi_n^{(1)} = 0. \tag{42}$$

Using the same argument as above we find that also the first order-correction $\psi_n^{(1)}$ is independent of the small-scale structure of $N(z)$. This correction is therefore a function $u_n^{(1)}(\alpha)$, which can be absorbed by the the zeroth-order solution $u_n^{(0)}(\alpha)$. eq. (36) then becomes

$$\left[\partial_\alpha^2 + \frac{N^2(\alpha,\beta)}{c_n^2}\right] u_n^{(0)}(\alpha) = -\partial_\beta^2\psi_n^{(2)}. \tag{43}$$

We decompose the buoyancy profile as follows

$$N^2(\alpha,\beta) = \Xi(\alpha) + \Omega(\beta), \tag{44}$$

where $\Xi(\alpha)$ is the slowly varying part of the buoyancy-frequency profile and $\Omega(\beta)$ the rapidly varying part. In order that $\Xi(\alpha)$ be uniquely defined, we impose the condition

$$\langle\Omega(\beta)\rangle = 0, \tag{45}$$

where $\langle\ldots\rangle$ denotes the average over the length scale β. Rewrite eq. (43) as

$$\left[\partial_\alpha^2 + \frac{\Xi(\alpha)}{c_n^2}\right] u_n^{(0)}(\alpha) = -\partial_\beta^2\psi_n^{(2)} - \frac{\Omega(\beta)}{c_n^2}u_n^{(0)}. \tag{46}$$

Because of the presence of $\Omega(\beta)$ on the right-hand side, eq. (46) shows that $\psi_n^{(2)}$ varies on the fast scale β. On this scale, the expression on the left-hand side is constant, and if this expression is non-zero it therefore gives rise to secular terms that are proportional to β^2. For $\psi_n^{(2)}$ to remain bounded as $\epsilon \to 0$ and $\beta \to \infty$, we must therefore require

$$\left[\partial_\alpha^2 + \frac{N^{h^2}(\alpha)}{c_n^2}\right] u_n^{(0)}(\alpha) \simeq 0, \tag{47}$$

where

$$N^{h^2}(\alpha) \equiv \langle N^2(\alpha,\beta)\rangle = \Xi(\alpha). \tag{48}$$

If Ω and therefore $\psi_n^{(2)}$ are strictly periodic in β, the average above is taken over one period, and the results are exact. However, they are also valid to a good approximation as long as there is a clear separation between the fast scale and the slow scale, that is, as long as ϵ is small. In this case, the average should be taken over a scale which is intermediate between the two scales, and the results do not depend on the details of the averaging. Note that in this case the variation of $u_n^{(0)}(\alpha)$ is constrained to be slower than that of $\Omega(\beta)$. If, on the other hand, there is no clear scale separation, it is uncertain whether one can define an average that makes the homogenization procedure valid.

The key result when applying the homogenization method is eq. (47), where we have transformed our problem (which originally depended upon two scales) into a one-scale problem, the fast β-dependent scale having been averaged out and reduced to a constant. The equation is valid as long as the variation of $u_n^{(0)}(\alpha)$ is slower than that of $\Omega(\beta)$. If we in addition assume that the variation of $u_n^{(0)}$ is more rapid than that of Ξ, eq. (47) can be solved by applying WKB theory. We will denote this combination of the WKB and homogenization techniques as the hybrid method. Under these circumstances the approximated wavefunction $u_n^{(0)}(\alpha)$ can be formulated as

$$u_n^{(0)}(\alpha) \simeq \sqrt{\frac{\overline{N^h}}{N(\alpha)}}\sin\left[\frac{n\pi}{H\overline{N^h}}\int_{-H}^{z} N^h(\alpha)\,\mathrm{d}\alpha\right]. \tag{49}$$

Hereafter application of the boundary conditions (26) yields the eigenvalue

$$c_n \simeq \frac{H\overline{N^h}}{n\pi} \tag{50}$$

as well as the wave number

$$\kappa_n \simeq \sqrt{\omega_0^2 - f_0^2}\,\frac{n\pi}{H\overline{N^h}}, \tag{51}$$

where

$$\overline{N^h} = \frac{\int_{-H}^{0} N^h(\alpha)\,\mathrm{d}\alpha}{H} \tag{52}$$

and the orthogonality relation becomes

$$\int_{-H}^{0}\psi_n(z)\psi_m(z)N^2(z)\,\mathrm{d}z \simeq \frac{\overline{N^h}^2 H}{2}\delta_{mn}. \tag{53}$$

We recognize that application of the homogenization theory leads to the following replacement scheme:

$$\overline{N} \;\to \overline{N^h}, \tag{54}$$

$$N_B \rightarrow N_B^h, \tag{55}$$

and the conversion rates

$$\mathcal{C}_n^h = \frac{\rho_0 U_0^2 L N_B^h}{2\pi}\sqrt{1-\frac{f_0^2}{\omega_0^2}}\tilde{h}(\kappa_n)\tilde{h}^*(\kappa_n)\kappa_n\delta\kappa. \tag{56}$$

Thus, when homogenization theory is applied, the conversion rates are not proportional to N_B, but to N_B^h, the latter being the homogenized bottom buoyancy frequency. For topographies with large horizontal length scale (i.e. large Λ), $n = 1, 2$ are the modes that carry most of the energy. The vertical length scale of these modes is the entire depth of the ocean, and N_B^h therefore depends on the stratification over the entire depth.

As above, we calculate the quotient between the conversion rates obtained using homogenization theory (alternatively the hybrid method if Ξ varies with α) and those determined numerically

$$R_n^h = \frac{\mathcal{C}_n^h}{\mathcal{C}_n^{\text{exact}}}. \tag{57}$$

Here we again need to integrate eq. (4) numerically to determine $\psi_n(-H)$. For the topography given by eq. (1), the sum of the modal conversion rates assumes the following form:

$$\mathcal{C}^h = \frac{\rho_0 U_0^2 h_0^2 L N_B^h \gamma}{2\pi}\sqrt{1-\frac{f_0^2}{\omega_0^2}}\Sigma_{n=1}^{\infty} n\gamma\exp(-2n\gamma), \tag{58}$$

where $\gamma = \Lambda\delta\kappa$.

Results for the infinite-depth case (viz. that associated with the continuous spectrum) are obtained by adhering to the same procedure as employed in Section 3

$$\mathcal{C}_{\text{Bell}}^h = \int_0^\infty \mathcal{C}_n^h \mathrm{d}\kappa = \rho_0 U_0^2 L N_B^h \sqrt{1-\frac{f_0^2}{\omega_0^2}}\int_0^\infty \tilde{h}(\kappa)\tilde{h}^*(\kappa)\kappa\,\mathrm{d}\kappa. \tag{59}$$

For the topography given by eq. (1), this yields

$$\mathcal{C}_{\text{Bell}}^h = \frac{\pi}{8}\rho_0 U_0^2 h_0^2 L N_B^h \sqrt{1-\frac{f_0^2}{\omega_0^2}}. \tag{60}$$

5. Results

In our model, we have used an ocean of finite depth $H = 4000$ m and a maximum height of the topography $h_0 = 400$ m. The shape of the topography is given by eq. (1), with different values of the ridge width Λ. The Coriolis parameter is taken to be $f_0 = 10^{-4}$ s^{-1}, the barotropic velocity $U_0 = 4 \times 10^{-2}$ m s^{-1}, the fundamental tidal frequency $\omega_0 = 2 \times 10^{-4}$ s^{-1}, and the unperturbed density $\rho_0 = 10^3$ kg m^{-3}. The outcome of the analyses will be reported in normalized form (i.e. $L = 1$ m), implying that $\mathcal{C}$ is the density of the conversion rates (W m^{-1}).

Figures 1 and 2 show two buoyancy-frequency profiles. The former is rather artificial, while the latter is an analytical construction resembling a real oceanic profile. We first consider the buoyancy-frequency profile, in Fig. 1, defined by

$$N^2(z) = \Xi(z) + N_2\sin(2\pi z/H\epsilon + \Delta\phi), \tag{61}$$

where $\Xi(z)$ is a slowly varying function

$$\Xi(z) = N_0 + N_1\sin(2\pi z/H). \tag{62}$$

Here $N_0 = 2 \times 10^{-5}$ s^{-2}, $N_1 = 10^{-6}$ s^{-2}, $N_2 = 10^{-5}$ s^{-2}, $\Delta\phi$ is a prescribed phase shift and $1/\epsilon = 10$. The buoyancy frequency at the seabed depends on the phase shift. For $\Delta\phi = 0$ we have $N_B = 4.472 \times 10^{-3}$ s^{-1}, and for $\Delta\phi = -\pi/2$ we have $N_B = 3.162 \times 10^{-3}$ s^{-1}. Moreover $N_B^h = 4.472 \times 10^{-3}$ s^{-1}. The criterion for the validity of linear wave theory is $N_B h/\Lambda\omega_0 < 1$. For example, when $\Delta\phi = -\pi/2$, $\Lambda > 6400$ m.

To proceed, we will employ the hybrid method. Thus, the homogenization technique will be used to take care of the rapidly

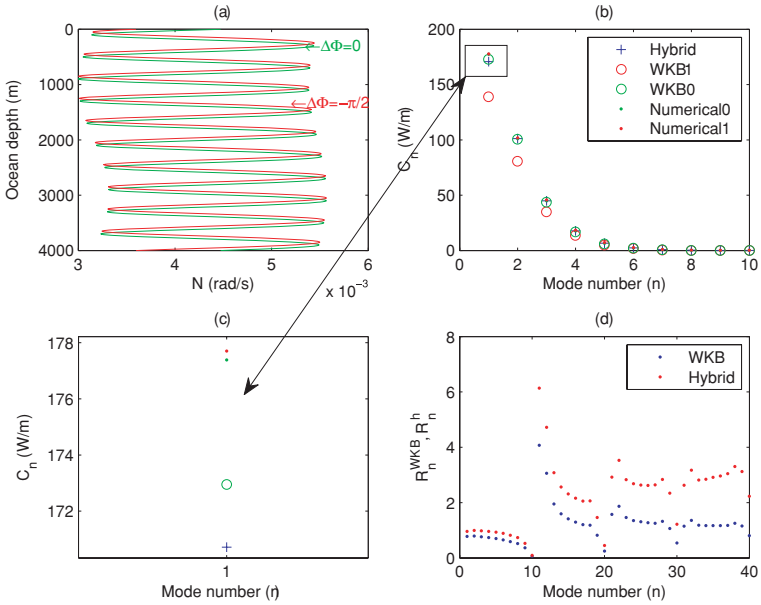

Fig. 1. (a) Two buoyancy profiles given by eq. (61). The green curve represents the case of $\Delta\phi = 0$ (case 0), the red $\Delta\phi = -\pi/2$ (case 1). (b) Dependence of the modal conversion rates upon the phase shift $\Delta\phi$, using $\Lambda = 20000$ m (crosses: hybrid-method results, rings: WKB solutions where $\Delta\phi = 0$ is green and $\Delta\phi = -\pi/2$ is red, filled circles: numerical solution). (c) "Blow-up" of the gravest-mode conversion rates. (d) Modal ratios R_n^{WKB} and R_n^h as functions of the mode number for $\Delta\phi = -\pi/2$.

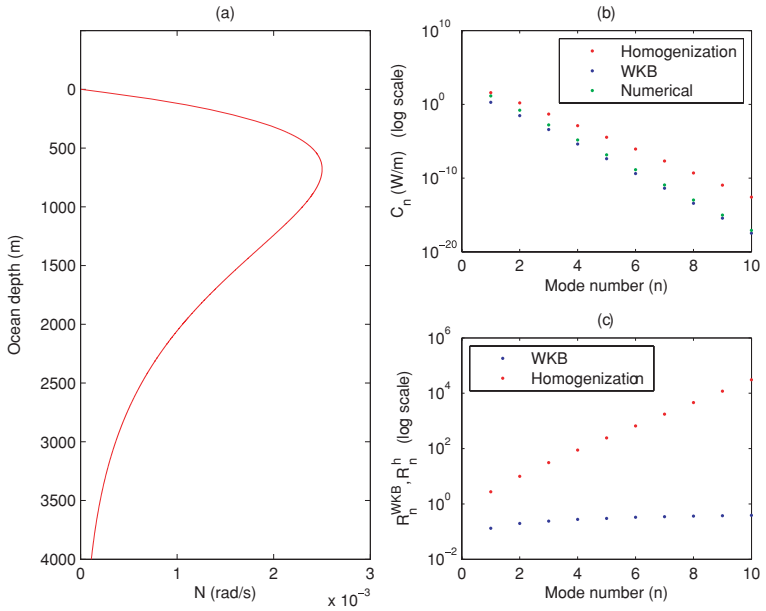

Fig. 2. (a) Realistic buoyancy-frequency profile given by eq. (63). (b) Modal conversion rates for $\Lambda = 20\,000$ m as functions of n obtained using the WKB technique (blue), the homogenization method (red), and numerical integration (green). (c) R_n^{WKB} (blue) and R_n^h (red) as functions of the mode number. Note that in panels b and c the vertical axis is logarithmically scaled.

varying part of the profile, with period ϵH, while WKB theory will be applied for dealing with the slow variations occurring over the length-scale of order H.

Figure 1b shows the dependence of the modal conversion rates $\mathcal{C}_n$ on the mode number n, setting $\Lambda = 20\,000$ m in eq. (1). The diagram includes results obtained using the WKB approximation, the hybrid technique and the purely numerical method. (Figure 1c shows the results obtained for $\mathcal{C}_1$ in greater detail.) From Figs. 1b and 1c it is seen that the correct values of the $\mathcal{C}_n$, which are obtained numerically, change only slightly when the value of N_B is changed by changing the phase shift $\Delta\phi$. The weakness of the WKB technique is revealed by the fact that the resulting $\mathcal{C}_n$ are highly sensitive to the phase shift, which in particular holds true for the gravest modes. The results obtained by the hybrid method, on the other hand, are by construction independent of this phase shift.

Figure 1d shows the ratios R_n^{WKB} and R_n^h (the previously introduced quotients between the approximated and 'exact' conversion rates) as functions of the mode number, using $\Delta\phi = -\pi/2$. For $n < 10$, the hybrid method gives better results than the WKB theory. Moreover, for the lowest modes, R_n^h is very close to unity, in contrast to R_n^{WKB}. For $n > 10$, R_n^h becomes larger and less accurate than R_n^{WKB}, it eventually diverges from unity whereas R_n^{WKB} approaches this value. It should furthermore be noted that both R_n^{WKB} and R_n^h show a resonance for mode numbers $n = 10 \times M$, $M = 1, 2, 3\ldots$. This occurs when the wavelength of the buoyancy frequency profile coincides with the wavelength of the internal wave.

The profile chosen in this first example is of course artificial, but it serves to illustrate an essential point. According to the WKB-approximation the conversion rate is proportional to N_B, the buoyancy-frequency at the bottom, but in the hybrid method N_B is replaced by N_B^h, the homogenized value at the bottom. The results above show that this gives good results as long as the vertical wavelength is longer than the period of the rapid variations in the buoyancy-frequency profile, which is true for the modes $n < 10$. For more realistic profiles the variations do not have a distinct scale, but the results above imply that reasonable results can then be obtained by homogenizing the profile over length scales shorter than the vertical wavelength. The problem is, of course, that the vertical wavelength near the bottom is unknown a priori.

In the second case (Fig. 2), we use the buoyancy-frequency profile

$$N^2(z) = N_0^2 + \left(\frac{N_1 z}{H}\right)^2 \exp(2z/\delta), \tag{63}$$

where $N_0 = 10^{-5}$ s^{-1}, $N_1 = 4 \times 10^{-2}$ s^{-1} and $\delta = 680$ m. The buoyancy frequency at the seabed is $N_B = 1.119 \times 10^{-4}$ s^{-1}. Linear theory is valid when $\Lambda > 224$ m. This profile qualitatively resembles a realistic profile, with N of the order 2×10^{-3} s^{-1} in the thermocline. In contrast to the previous profile, this one is not periodic, and does not have two distinct scales. We will proceed by averaging the profile over the entire ocean depth, hence, the homogenized buoyancy frequency is obtained as follows:

$$N^{h2} = N_0^2 + \left\langle \left(\frac{N_1 z}{H}\right)^2 \exp(2z/\delta) \right\rangle = constant, \tag{64}$$

with $N^h = 1.401 \times 10^{-3}$ s^{-1}. This will be seen to give good results for at least the gravest mode, whose scale is also of the same order as the entire ocean depth.

Figure 2b shows the logarithm of the resulting modal conversion rates $\mathcal{C}_n$ as a function of the mode number, with $\Lambda = 20\,000$ m in eq. (1). As in the previous case, the conversion rates

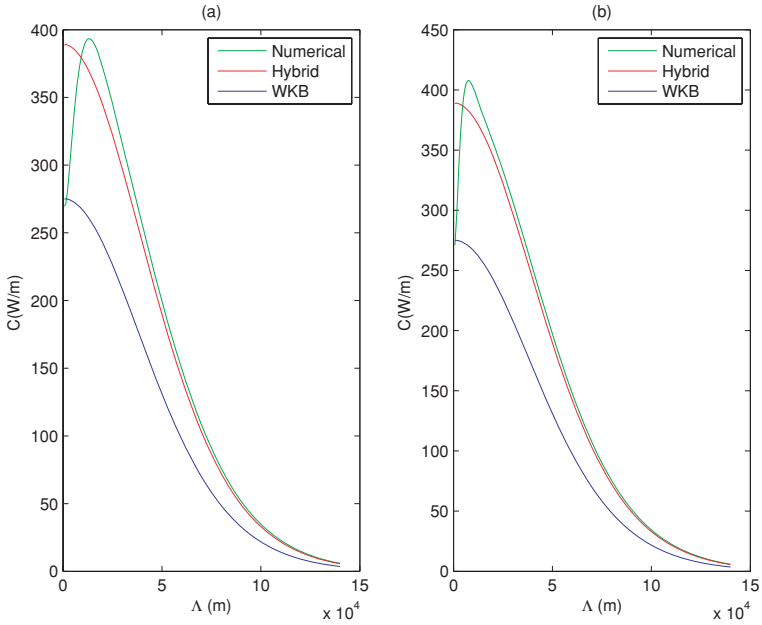

Fig. 3. (a) Total conversion rates $\mathcal{C}$ as function of the ridge width Λ for the oscillating buoyancy frequency profile for $\Delta\phi = -\pi/2$ in Fig. 1. WKB, hybrid-method, and numerical results are blue, green, red, respectively. (a) $1/\epsilon = 5$ (b) $1/\epsilon = 10$.

decrease exponentially with increasing values of n. The numerically calculated $\mathcal{C}_n$ are close to those based on homogenization theory for $n = 1$ and approach the WKB results for higher modes. Figure 2c shows the ratios R_n^{WKB} and R_n^h as logarithmic functions of n. Here R_n^{WKB} tends asymptotically towards unity for increasing values of n, but is of magnitude 0.1 for the gravest modes. R_n^h is of order unity for the gravest mode but diverges from this value for the higher modes.

Figures 3 and 4 show the total conversion rate $\mathcal{C}$ (obtained by summing $\mathcal{C}_n$ over the entire spectrum) as a function of the horizontal scale Λ of the topography. The results are shown for both buoyancy frequency profiles, as specified by eqs (61) and (63), respectively, where the former is phase shifted by $\Delta\phi = -\pi/2$. The diagrams include results based on the numerical solution, the hybrid/homogenization procedure, and the WKB method. For $\Lambda \to 0$, that is, a narrow ridge, the results obtained using WKB theory are nearly identical to those determined numerically. As Λ increases, the numerical results approach those obtained using the hybrid/homogenization method, cf. Figs. 3 and 4b.

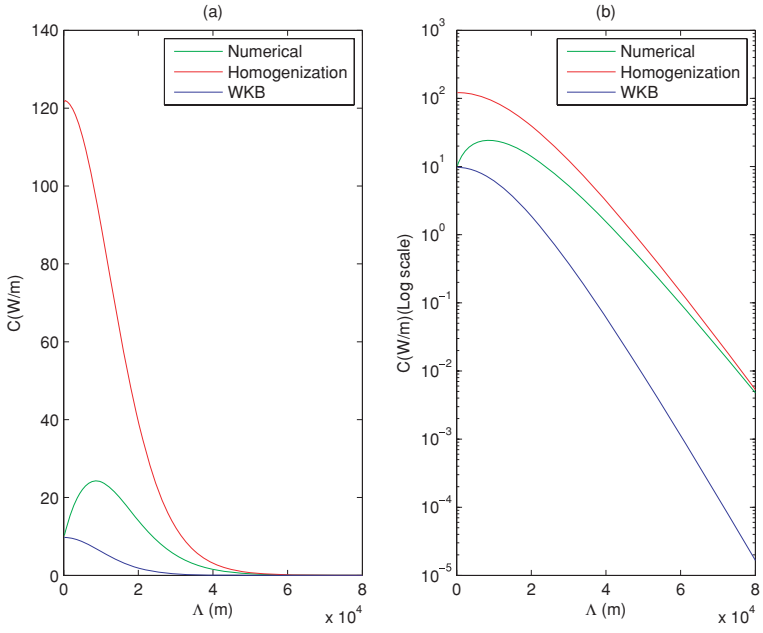

Fig. 4. (a) Total conversion rates $\mathcal{C}$ as functions of the ridge width Λ for the realistic buoyancy-frequency profile in Fig. 2. WKB, homogenization-method, and numerical results are blue, green and red, respectively. (b) Logarithmically scaled version of the results in panel a.

For the profile in Fig. 1a, the transition from the WKB-curve to the one obtained with the hybrid method occurs at a fairly distinct value of Λ, which depends on the scale of the rapid variations in the buoyancy frequency profile. This is illustrated by the two cases shown in Fig. 3, which have $1/\epsilon = 5$ and $1/\epsilon = 10$, respectively. For the more realistic profile in Fig. 2a, there is also a transition from the WKB-curve to the one obtained with the hybrid method, although it occurs at a less distinct value of Λ. Since the average of N^2 over the whole water column is always much larger than the value at the bottom, the conversion calculated with the homogenisation method is larger than when using the WKB-approximation. The result is that the largest conversion is obtained at the transition from the WKB-curve to the homogenisation curve; in this example for a ridge width Λ of the order 10 km. This is in marked contrast to the previous results obtained either by using the WKB approximation or by assuming a constant buoyancy frequency (Llewellyn Smith and Young, 2002). In both these cases, the largest conversion is obtained in the limit $\Lambda \to 0$, that is, for a very narrow ridge.

6. Discussion

In this study, the energy conversion rate for tidally generated internal waves has been calculated both numerically and using two different approximate methods. It was demonstrated that the traditional WKB method, which is accurate for higher-mode waves (or, equivalently, for 'narrow-ridge' topography), is not applicable to the gravest wave modes. Another method, the homogenization technique, was therefore introduced. This method was shown to be accurate for the gravest modes (or, equivalently, for 'broad-ridge' topography). The two methods therefore complement each other.

A particular weakness of the WKB method is that it yields an energy conversion rate that is proportional to the seabed buoyancy frequency N_B. Since N_B can be very small due to localised mixing near the bottom, this may give large errors. A better result is obtained if N_B is replaced by N_B^h, that is, if we homogenize the buoyancy frequency over a vertical wavelength. The result is then insensitive to the precise value of N_B. For the gravest mode this means homogenizing over the entire water column, which gives a much larger value than N_B.

We have studied how the energy conversion at a bell-shaped ridge depends on its width Λ. If the WKB approximation is used, or if the buoyancy-frequency is assumed to be constant, the energy conversion decreases monotonically as Λ increases (Llewellyn Smith and Young, 2002). This effect is caused by the finite depth, because of which the internal waves have a maximal horizontal wavelength. If the topography is broader than this wavelength, it projects weakly on the internal modes. The numerical calculations with a realistic buoyancy-frequency profile in this study have demonstratred that this effect is counteracted by another effect, which tends to increase the energy conversion with increasing Λ. It is caused by the fact that for the lower modes excited with a broader topography, the buoyancy frequency should effectively be homogenized over a larger vertical scale, giving a larger value of N_B^h.

As a result of these conflicting tendencies, the energy conversion reaches a maximum at some intermediate value of Λ. In the realistic example presented here, this occurs for a ridge width of about 10 km, and the energy conversion for this width is roughly three times greater than the value obtained with the WKB approximation. This may mean that the computation of the global energy conversion by Nycander (2005), which was based on the WKB approximation, gives too low values.

The homogenization technique has here been introduced as a tool for understanding the qualitative effect of the density profile, rather than as a method for practical computations. To be valid, the method requires a distinct scale separation, which is rarely present in reality. In computations of the full solution, based on an expansion in the infinite series of vertical eigenmodes, it is probably best to compute the eigenmodes numerically, rather than using either the WKB-approximation or the homogenization technique.

Nevertheless, it is conceivable that homogenization could provide a way of improving the simple and approximate method used by Nycander (2005) for global computations, which avoids the expansion in eigenmodes. The homogenization technique would then be used for long topographic scales, while the WKB-approximation would still be used for short scales. However, it remains to be seen whether this idea is feasible.

7. Acknowledgments

We acknowledge hereby the decisive contribution of our reviewers to the amelioration of the original version of the manuscript.

References

Alford, M. H. 2003. Redistribution of the energy available for ocean mixing by long-range propagation of internal waves. *Nature* **423**, 159–162.

Andrews, J. C. and Gentien, P. 1982. Upwelling as a source of nutrients for the Great Barrier Reef ecosystem: a solution to Darwin's question? *Mar. Ecol. Prog. Ser.* **8**, 257–269.

Bell, T. H. 1975a. Lee waves in stratified flows with simple harmonics time dependence. *J. Fluid Mech.* **67**, 705–722.

Bell, T. H. 1975b. Topographically generated internal waves in the open ocean. *J. Geophys. Res.* **80**(3), 320–327.

Bender, C. M. and Orszag, S. A. 1978. *Advanced Mathematical Methods for Scientists and Engineers*, McGraw-Hill, New York.

Egbert, G. D. and Ray, R. 2000. Significant dissipation of tidal energy in the deep ocean inferred from satellite altimeter data. *Nature* **405**, 775–778.

Egbert, G. D. and Ray, R. 2001. Estimates of M_2 tidal energy dissipation from TOPEX/POSEIDON altimeter data. *J. Geophys. Res.* **106**(C10), 22475–22502.

Khatiwala, S. 2003. Generation of internal tides in an ocean of finite depth: analytical and numerical calculations. *Deep Sea Res. I,* **50**, 3–21.

Ledwell, J. R., Montgomery, E. T., Polzin, L. T., St. Laurent, L. C., Schmitt, R. W., and co-authors. 2000. Evidence for enhanced mixing over rough topography in the Abyssal Ocean. *Nature* **403**, 179–182.

Leichter, J. J., Shellenbarger, G., Genovese, S. J. and Wing, S. R. 1998. Breaking internal waves on a Florida (USA) coral reef: a plankton pump at work? *Mar. Ecol. Prog. Ser.* **166**, 83–97.

Llewellyn Smith, S. G. and Young, W. R. 2002. Conversion of the Barotropic tide. *J. Phys. Oceangr.* **32**, 1554–1566.

Morse, P. and Feshbach, H. 1953. *Methods of Theoretical Physics*, McGraw-Hill, New York.

Munk, W. and Wunsch, C., 1998. Abyssal recipes II: energetics of tidal and wind mixing. *Deep-Sea Res. I,* **45**, 1977–2010.

Nilsson, J., Broström, G. and Walin, G. 2003. The thermohaline circulation and vertical mixing: does weaker density stratification give stronger overturning? *J. Phys. Oceanogr.* **33**, 2781–2795.

Nycander, J. 2005. Generation of internal waves in the deep ocean by tides. *J. Geophys. Res.* **101**, C10028, doi:10.1029/2004JC002487.

Sandström, J. W. 1908. Dynamishe Versuche mit Meerwasser. *Annals in Hydrodynamic Marine Meteorology*. **36,** 6–23.